COMPUTED TOMOGRAPHY

Prognostic analysis and risk stratification of lung adenocarcinoma undergoing EGFR-TKI therapy with time-serial CT-based radiomics signature

Xiaobo Zhang[1] · Bingfeng Lu[2] · Xinguan Yang[3] · Dong Lan[4] · Shushen Lin[5] · Zhipeng Zhou[6] · Kai Li[1] · Dong Deng[1] · Peng Peng[1] · Zisan Zeng[1] · Liling Long[1] ◉

Abstract

Objectives To evaluate the value of time-serial CT radiomics features in predicting progression-free survival (PFS) for lung adenocarcinoma (LUAD) patients after epidermal growth factor receptor-tyrosine kinase inhibitors (EGFR-TKIs) therapy.

Materials and methods LUAD patients treated with EGFR-TKIs were retrospectively included from three independent institutes and divided into training and validation cohorts. Intratumoral and peritumoral features were extracted from time-serial non-contrast chest CT (including pre-therapy and first follow-up images); moreover, the percentage variation per unit time (day) was introduced to adjust for the different follow-up periods of each patient. Test-retest was performed to exclude irreproducible features, while the Boruta algorithm was used to select critical radiomics features. Radiomics signatures were constructed with random forest survival models in the training cohort and compared against baseline clinical characteristics through Cox regression and nonparametric testing of concordance indices (C-indices).

Results The training cohort included 131 patients (74 women, 56.5%) from one institute and the validation cohort encompassed 41 patients (24 women, 58.5%) from two other institutes. The optimal signature contained 10 features and 7 were unit time feature variations. The comprehensive radiomics model outperformed the pre-therapy clinical characteristics in predicting PFS (training: 0.78, 95% CI: [0.72, 0.84] versus 0.55, 95% CI: [0.49, 0.62], $p < 0.001$; validation: 0.72, 95% CI: [0.60, 0.84] versus 0.54, 95% CI: [0.42, 0.66], $p < 0.001$).

Conclusion Radiomics signature derived from time-serial CT images demonstrated optimal prognostic performance of disease progression. This dynamic imaging biomarker holds the promise of monitoring treatment response and achieving personalized management.

Key Points

• *The intrinsic tumor heterogeneity can be highly dynamic under the therapeutic effect of EGFR-TKI treatment, and the inevitable development of drug resistance may disrupt the duration of clinical benefit. Decision-making remained challenging in practice to detect the emergence of acquired resistance during the early response phase.*

• *Time-serial CT-based radiomics signature integrating intra- and peritumoral features offered the potential to predict progression-free survival for LUAD patients treated with EGFR-TKIs.*

• *The dynamic imaging signature allowed for prognostic risk stratification.*

Keywords Radiomics · Lung adenocarcinoma · EGFR-TKI · Time-serial computed tomography · Peritumoral feature

---

Xiaobo Zhang, Bingfeng Lu, and Xinguan Yang have contributed equally to this work and share first authorship.

✉ Liling Long
  cjr.longliling@vip.163.com

1 Department of Radiology, The First Affiliated Hospital of Guangxi Medical University, No.6 Shuangyong Road, Qingxiu District, Nanning 530021, Guangxi, China

2 Department of Radiology, The Second Affiliated Hospital of Guangxi Medical University, Nanning, Guangxi, China

3 Department of Radiology, Guilin People's Hospital, Guilin, Guangxi, China

4 Department of Oncology, The First Affiliated Hospital of Guangxi Medical University, Nanning, Guangxi, China

5 Siemens Healthineers, Shanghai, China

6 Department of Radiology, Affiliated Hospital of Guilin Medical University, Guilin, Guangxi, China

⚫ Springer

Abbreviations

3D	Three-dimensional
AIC	Akaike information criterion
AUC	Areas under the curve
CI	Confidence interval
C-index	Concordance index
EGFR	Epidermal growth factor receptor
HIS	Hospital Information System
ICC	Interclass correlation coefficient
IQR	Interquartile ranges
LUAD	Lung adenocarcinoma
NCCN	National comprehensive cancer network
NSCLC	Non-small cell lung cancer
PACS	Picture Archiving and Communication Systems
PFS	Progression-free survival
R-group	Rapid progression group
ROC	Receiver operating characteristic
S-group	Slow progression group
TKI	Tyrosine kinase inhibitor
VOI	Volume of interest

Introduction

Epidermal growth factor receptor (EGFR) is one of the most targeted driver genes, and its activating mutation is especially prevalent in the Eastern Asian lung adenocarcinoma (LUAD) population [1]. Many studies demonstrated that LUAD patients harboring EGFR mutations could benefit from EGFR tyrosine kinase inhibitor (TKI) therapy, which compared to chemotherapy alone would prolong progression-free survival (PFS) [2–6]. However, most of these patients eventually develop progression due to the acquired resistance to EGFR TKIs within 1 year after the initiation of targeted treatment [3–6]. Therefore, accurately predicting disease progression and early identifying patients whose drug resistance developed rapidly are crucial to optimize follow-up strategy and guide subsequent treatment.

Re-biopsy at the targeted lesion is the main method to determine secondary resistance [7, 8]. However, the application of re-biopsy is limited in clinical practice for many reasons including its invasiveness, limited tissue availability [9, 10] and ambiguous timing of such examination [9, 11]. As the result, early prediction and detection of acquired resistance remain challenging.

Radiomics emerged as a popular image analysis method in the past decade, enabling high-throughput feature extraction to quantitatively describe tumor heterogeneity [12–14]. Previous lung cancer studies applied radiomics to differential diagnosis [15, 16], treatment response [17–19], prognostic prediction [20–26], estimation of tumor phenotype [19] and mutation status [27–30]. Most radiomics-based studies have predominantly investigated the association between clinical outcomes and intra-tumoral radiomics features at a single timepoint. For example, Song et al indicated radiomics features extracted from pretherapy CT images had a considerable value on prediction of PFS for stage IV EGFR-mutant non-small cell lung cancer (NSCLC) patients who received EGFR-TKI therapy [20]. However, few studies focused on the prognostic value of radiomics features at multiple timepoints throughout EGFR-TKI therapy for LUAD patients with EGFR mutation [19, 21, 24, 31] or considered the prognostic impact of peritumoral tissue [26]. Fave et al concluded that delta-radiomics features could provide better patient-specific outcome predictions compared with pretreatment features [24]. Meanwhile, Dou et al identified peritumoral radiomics features as significant indicators of distant metastasis in locally advanced NSCLC [26]. Therefore, our study aimed to explore whether a radiomics signature encompassing intra- and peri-tumoral radiomics features from time-serial CT can accurately predict PFS and early stratify the risk of acquired resistance for lung adenocarcinoma patients undergoing EGFR-TKI treatment.

Materials and methods

Patient selection

Two hundred and nine lung adenocarcinoma patients who were treated with EGFR TKIs according to the criteria established by the National Comprehensive Cancer Network (NCCN) at three independent institutes between January 1, 2015 and September 30, 2020 were evaluated. The clinical characteristics, such as sex, age, ethnicity, smoking status, administered targeted drug, and TNM stage, were recorded from Hospital Information System (HIS) for all eligible patients. Patients' serial CT data were obtained from Picture Archiving and Communication Systems (PACS). Inclusion criteria were as follows: (1) histologically confirmed lung adenocarcinoma; (2) received EGFR TKI monotherapy till disease progressed; (3) underwent baseline chest CT scans within 8 weeks before the EGFR-TKI therapy and at least one follow-up CT scan before disease progressed; (4) at least one measurable targeted lesion (≥ 10 mm) at baseline CT imaging. Exclusion criteria were as follows: (1) Patients with history of surgery resection; (2) incomplete clinical data; (3) targeted lesions unable to be segmented (e.g. lesions adjacent to atelectasis or diffuse lesions). A flow chart of patient selection is illustrated in Fig. 1.

CT examinations, follow-up strategy, and disease progression

All those who were eligible underwent baseline chest CT scans within 8 weeks before the EGFR-TKI therapy. The
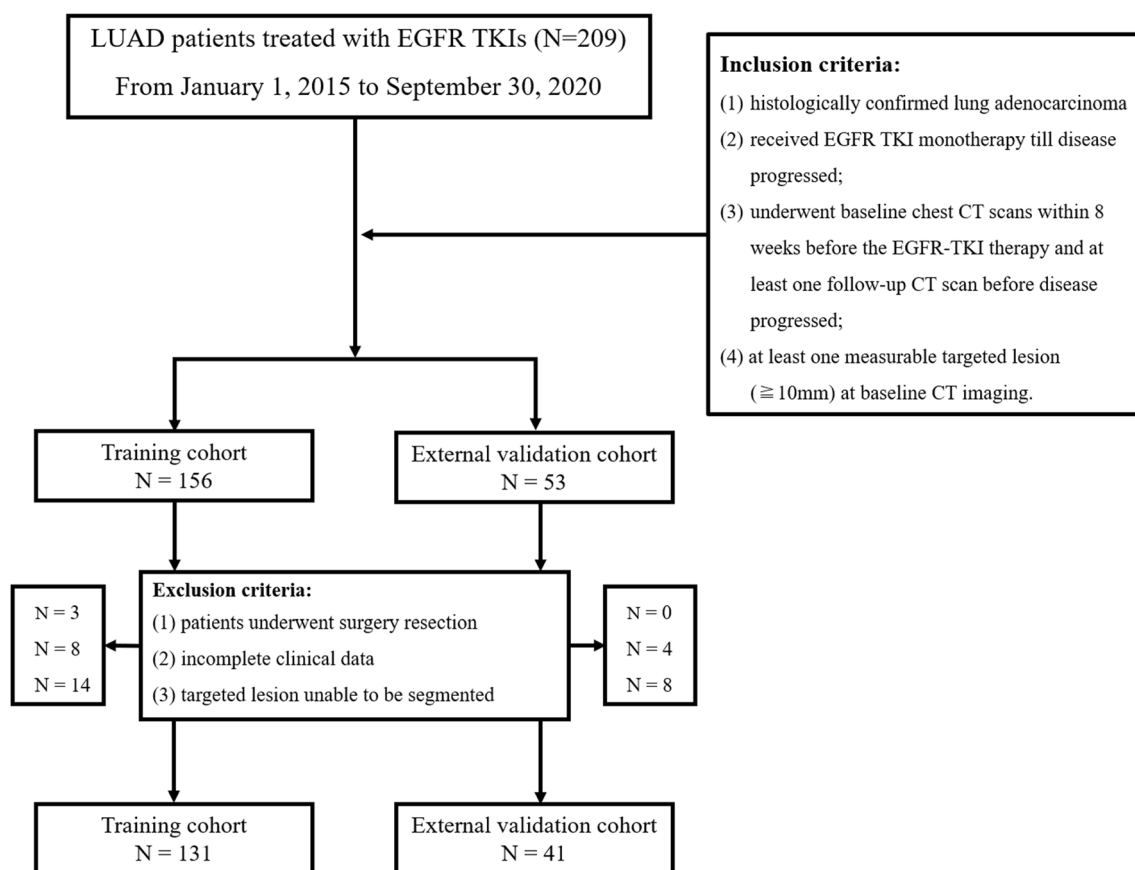
Fig. 1 Flow chart of patient selection with inclusion and exclusion criteria

follow-up interval was every 6–12 weeks according to NCCN guidelines, wherein the first follow-up for response assessment was performed 6 weeks after initiation of therapy. A portion of patients (30/172, 17.4%) didn't undergo imaging scans at that timepoint. Therefore, the first follow-up CT scan images before disease progression occurred were analyzed.

The response to EGFR-TKI treatment was assessed according to Hayes' criteria [32] and RECIST version 1.1 [33]. Disease progression was determined as the volume of targeted lesion increased by 20% or the appearance of new lesions. The primary endpoint of this study is disease progression, and PFS was defined as the duration from initiation of EGFR-TKI therapy to disease progression. Death, loss to follow-up, and non-occurrence of outcome were properly censored.

The chest CT examinations were performed with multi-vendor multi-systems at the three institutes. Details regarding the acquisition and reconstruction parameters are presented in Table S1.

Radiomics feature extraction

Three-dimensional (3D) volumes of interest (VOIs) of primary lesion at baseline (F0) and first follow-up (F1) were segmented semi-automatically by a radiologist with 21 years of experience in chest CT interpretation in a research workstation (Syngo.via Frontier, Radiomics, version 1.2.5, Siemens Healthineers). The radiologist delineated the primary pulmonary lesions in three-dimensional space, and then defined two peritumoral rings ($peri_{5mm}$ and $peri_{10mm}$) based on segmented tumor contour by dilating the lesion borders by 5 mm and 10 mm, respectively (Fig. 2). After border dilation, the radiologist paid close attention to avoid the peritumoral regions from breaching into the chest wall or lung mediastinum and manually modified the segmentations if necessary. Baseline tumor volumes were also recorded from segmentation. The $peri_{5mm}$ ring was obtained by subtracting the region of the primary tumor from the region of $dilation_{5mm}$. In the same way, the $peri_{10mm}$ ring was generated by subtraction between the region of $dilation_{5mm}$ and $dilation_{10mm}$. For each segmented region, the prototypical software outputted 1691 radiomics features based on intensity, shape, and texture characteristics (Table S2). To ensure the reliability and reproducibility of the extracted features, the same radiologist performed test-retest analysis by conducting segmentations on 30 randomly chosen patients a month apart from the initial evaluation. The interclass correlation coefficient (ICC) greater than 0.80 was considered as excellent reliability and subsequently used to exclude features with low intra-observer agreement. Finally, the remaining features were compared between baseline and first follow-up to compute the
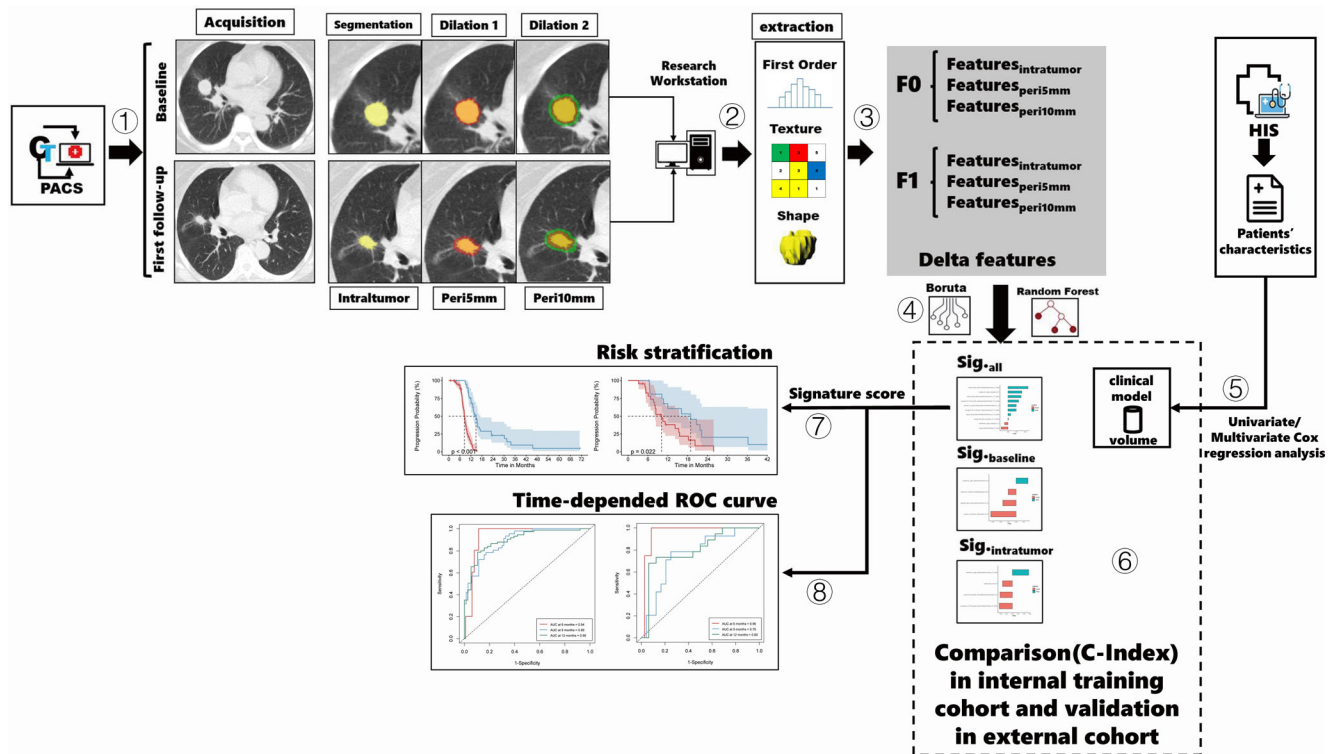
Fig. 2 Study workflow. Step 1: Serial CT images including baseline and first follow-up were acquired and segmented. Primary tumor and its peritumoral rings were semi-automatically delineated and manually confirmed. Step 2: Radiomics features based on first-order, shape and texture characteristics were extracted from each segmented region through a prototypical software. Step 3: Test-retest was performed to select stable features with ICC > 0.8 and subsequently compute delta features. Step 4: Feature selection from internal training cohort was conducted with Boruta algorithm to formulate optimal radiomics signatures through random forest survival models. Step 5: Univariate and multivariate Cox regression analysis was performed with all clinical factors and a clinical model was established. Step 6: The progression-predictive performance between models was compared in training cohort and validated in external cohort. Step 7: Risk stratification with the best-performing radiomics signature. Step 8: Time-depended ROC curve was used to evaluate the accuracy of prediction at different time points

percentage variation per unit time (Eq. 1, where $Diff_{time}$ refers to the time difference between two CT scans).

Equation 1 Percentage variation per unit time (day)

$$Delta_{radiomics} = \frac{1}{Diff_{time}} \cdot \frac{Radiomics_{F1} - Radiomics_{F0}}{Radiomics_{F0}} \quad (1)$$

Feature selection and radiomics signature construction

The stable features from baseline, first follow-up, and between-scan variation from the internal training cohort underwent feature selection process with the Boruta algorithm. This algorithm iteratively wrapped around random forest survival analyses to explore all possible subsets of the attributes and finally selects the most important features related to PFS by comparing the importance of the original attributes with the importance achievable at all permutations [34, 35]. Based on the sample size of the training cohort, the ten most important features were refined to build the

optimal random forest survival model and obtain the radiomics signature (model_all) of each patient. Meanwhile, the same feature selection and modeling processes were repeated with baseline imaging features alone (model_baseline) and intratumoral features alone (model_intratumor) to understand the added value of the time-serial radiomics features and peritumoral features.

Risk stratification and prognostic accuracy

LUAD patients were stratified into rapid or slow progression subgroups using the cutoff radiomics signature score determined in the training cohort by maximally selected Log-Rank statistics. The Kaplan-Meier analysis was performed in both training and external validation cohorts to identify the clinical efficacy of our proposed radiomics signature. The prognostic accuracy of the signature at different timepoints was evaluated by the time-dependent receiver operating characteristic (ROC) curve. ROC curves at the 6th, 9th, and 12th months were plotted for both cohorts respectively and the corresponding areas under the curve (AUC) were calculated.

Statistical analysis

Baseline demographic and clinical characteristics were expressed in means ± standard deviations, medians with interquartile ranges (IQR), and frequencies (percentages) based on normality and continuous nature of the variable. Chi-square test and Wilcoxon's two-sample test were deployed to compare the patient characteristics between the internal training cohort and the external validation cohort. Cox regression models were built for each radiomics signature to evaluate their PFS-predicting performance. Meanwhile, the clinical parameters underwent a univariate Cox regression analysis and a forward selecting multivariate Cox regression analysis, and the clinical model ($model_{clinical}$) was constructed with the selected variables. Akaike information criterion (AIC) was adopted to screen the optimal clinical model. The model containing the fewest parameters with the lowest AIC value is the most optimal model. Additionally, the best-performing radiomics signature was combined with the clinical model to achieve a clinico-radiomics prediction ($model_{combined}$). Harrell's concordance index (C-Index) in both training and validation cohorts were calculated and compared via a pairwise nonparametric test among radiomics and clinical and combined models. All statistical analyses were conducted using R software (version 3.6.0, http://www.Rproject.org).

Results

Patient characteristics

A total of 172 eligible patients were enrolled in this study according to our criteria. A hundred and thirty-one patients from the institute A were designated as the training cohort (74 females, 56.5%). The remanent 41 patients from the other two independent hospitals (24 from institute B and 17 from institute C, respectively) consisted of the external validation cohort (24 females, 58.5%).

There was no significant difference in PFS between the two cohorts (median PFS: training cohort, 11.1 months; validation cohort, 13.1 months; $p = 0.199$). A hundred and forty-two of 172 (83%) patients developed disease progression during the follow-up period (109 patients in the training set, 33 patients in the external validation set). Fifteen of 172 (9%) patients didn't progress (13 patients in the training set, 2 patients in the validation set) and 15 (9%) patients were lost to follow-up (9 patients in the training set, 6 patients in the validation set). The minimum first follow-up period was 16 days after therapy; while the maximum first follow-up time was 128 days (median: 35 days).

Furthermore, the two cohorts exhibited similar baseline clinical characteristics except for volume at baseline ($p =$

0.011). Details on the patient's characteristics as well as data available are provided in Table 1.

Univariate and multivariate Cox regression

A univariate Cox regression analysis performed with all clinical factors indicated volume at baseline (HR: 1.006, CI: 1.000, 1.013, $p = 0.045$) as statistically significant to the prediction of disease progression (Table 2). Besides, other characteristics, such as sex, age, smoking status, TNM stage, etc., did not show significant prognostic impact. The clinical model constructed by baseline volume was the optimal model with the lowest AIC value (850.63).

Radiomics feature selection

In the training cohort, we extracted 6 sets of radiomics features from the intratumoral and peritumoral region (including $peri_{5-mm}$ ring and $peri_{10mm}$ ring) at baseline and first follow-up CT scan, respectively. Each set comprised 1691 features that included 17 shape features, 324 first-order features, and 1350 texture features. The test-retest analysis refined the number of features to 6578 (each timepoint included 1162 intratumoral features, 1068 $peri_{5mm}$ features and 1059 $peri_{10mm}$ features). The baseline, follow-up, and delta radiomics features underwent the Boruta selection algorithm, and the ten most important features were combined for the final PFS-predicting signature using the random forest survival model. Among these features, 6 texture features, 3 shape-based, and one first-order feature were representatives. In terms of extraction location and time phase, 8 features were obtained from the peritumoral region and delta radiomics features accounted for 70% of the top 10 features.

Model performance

The $model_{all}$ for predicting PFS achieved the C-Index of 0.78 (95% CI: 0.72, 0.84) in the training cohort and 0.72 (95% CI: 0.60, 0.84) in the external validation cohort. The C-index yielded from the $model_{clinical}$ was 0.55 (95% CI: 0.49, 0.62) in the training cohort and 0.54 (95% CI: 0.42, 0.66) in the validation cohort, which was both significantly lower than those of the $model_{all}$ ($p < 0.001$). The combined clinico-radiomics model achieved the C-Index of 0.77 (95% CI: 0.71, 0.84) in the training cohort and 0.72 (95% CI: 0.60, 0.84) in the validation cohort. The composite model indicated no incremental benefit in progression prediction of both cohorts ($p = 0.713, 0.756$ respectively). The C-Index of the $model_{baseline}$ (training cohort: 0.66, 95% CI:0.60, 0.73; validation cohort: 0.57, 95% CI:0.50, 0.69) and the C-Index of the $model_{intratumor}$ (training cohort: 0.71, 95% CI:0.65, 0.78; validation cohort: 0.65, 95% CI:0.53, 0.77) were both numerically inferior to the comprehensive model. The comprehensive

Table 1 Demographic and clinicopathologic characteristics

	Training ($n = 131$)	External ($n = 41$)	p value
Sex			0.960
Female	74 (56.5%)	24 (58.5%)	
Male	57 (43.5%)	17 (41.5%)	
Age			1.000
< 60	70 (53.4%)	22 (53.7%)	
≥ 60	61 (46.6%)	19 (46.3%)	
Smoking status			0.831
No	98 (74.8%)	32 (78.0%)	
Yes	33 (25.2%)	9 (22.0%)	
Ethnicity			0.246
Han Chinese	74 (56.5%)	28 (68.3%)	
Minority Chinese	57 (43.5%)	13 (31.7%)	
Tumor size (mm^3)	29.7 (29.3)	20.2 (16.7)	0.011
T stage			0.089
I	5 (3.82%)	5 (12.2%)	
II	8 (6.11%)	4 (9.76%)	
III	16 (12.2%)	7 (17.1%)	
IV	102 (77.9%)	25 (61.0%)	
N stage			0.824
N0	16 (12.2%)	3 (7.32%)	
N1	34 (26.0%)	10 (24.4%)	
N2	48 (36.6%)	18 (43.9%)	
N3	33 (25.2%)	10 (24.4%)	
M stage			0.672
M0	5 (3.82%)	2 (4.88%)	
M1	126 (96.2%)	39 (95.1%)	
Clinical stage			0.462
I	0	0	
II	1	1	
III	1	1	
IV	129	39	
EGFR mutation status			0.729
Exon 19 deletion	62	20	
Exon 21 L858R	47	15	
Exon 18	4	0	
Exon 20	2	0	
EGFR+*	16	6	
TKI treatment			0.067
Afatinib	4 (3.05%)	1 (2.44%)	
Erlotinib	5 (3.82%)	1 (2.44%)	
Gefitinib	82 (62.6%)	17 (41.5%)	
Icotinib	33 (25.2%)	20 (48.8%)	
Osimertinib	7 (5.34%)	2 (4.88%)	
PFS	11.1 (8.22)	13.1 (8.43)	0.199

*Specific EGFR mutant type unknown

Table 2 Univariate Cox regression analysis of clinical characteristics

	Hazard ratio	Confidence interval	p value
Sex			
Female	Ref		
Male	0.980	0.665, 1.445	0.920
Age			
< 60	Ref		
≥ 60	0.999	0.6853, 1.456	0.996
Smoking status			
No	Ref		
Yes	1.105	0.720, 1.696	0.648
Ethnicity			
Han Chinese	Ref		
Minority Chinese	0.810	0.555, 1.184	0.278
Tumor size (mm^3)	1.006	1.000, 1.013	0.045
T stage			
I	Ref		
II	3.352	0.703, 15.98	0.129
III	2.518	0.571, 11.11	0.223
IV	1.696	0.416, 6.92	0.462
N stage			
N0	Ref		
N1	1.669	0.847, 3.292	0.139
N2	1.881	0.961, 3.683	0.065
N3	1.423	0.706, 2.869	0.324
M stage			
M0	Ref		
M1	0.453	0.142, 1.447	0.181
TKI treatment			
Afatinib	Ref		
Erlotinib	0.299	0.057, 1.575	0.154
Gefitinib	0.541	0.132, 2.223	0.394
Icotinib	0.540	0.127, 2.298	0.405
Osimertinib	0.182	0.025, 1.297	0.089

signature statistically outperformed the baseline and intratumoral signatures in the training cohorts ($p < 0.001$ and $p = 0.006$, respectively) but failed to reach statistical significance in the external validation cohort ($p = 0.086$ and $p = 0.198$, respectively) due to a limited sample size. The results of the model comparison were displayed in Fig. 3.

Risk stratification and prognostic accuracy

The log-rank statistics determined the optimal cutoff value of 49.86 (Figure S1) and divided the patients into rapid and slow progression subgroups (Fig. 4A, B). In both cohorts, the rapid progression group (median PFS: training cohort, 8.3 months; validation cohort, 9.1 months) had a shorter PFS than the slow
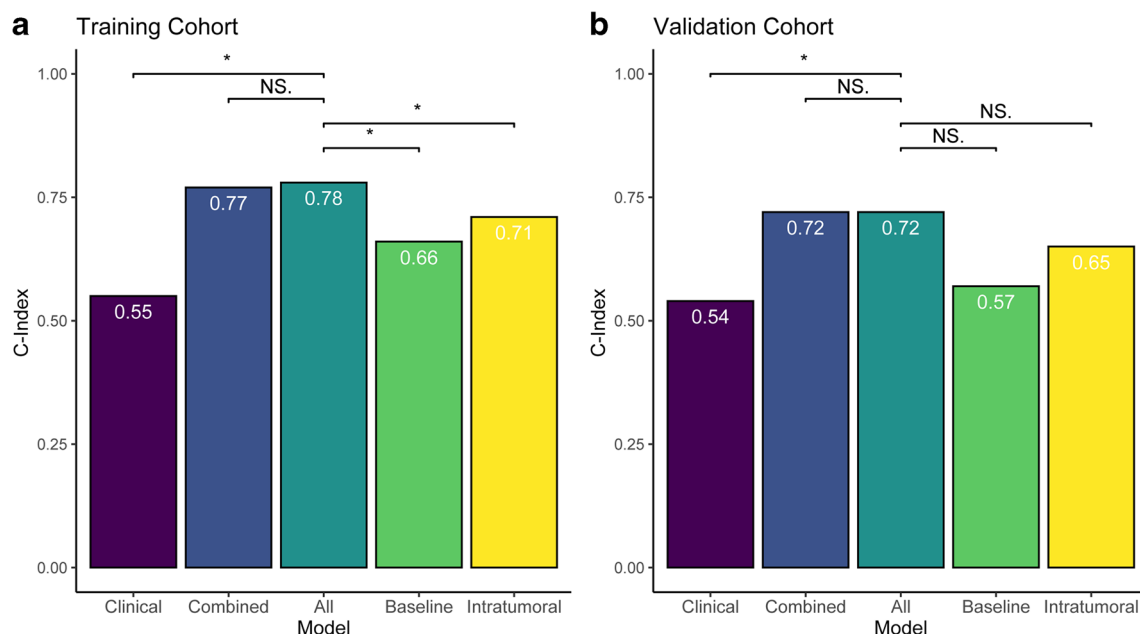
Fig. 3 Model performance within training (**a**) and validation (**b**) cohorts. C-indices were compared among models. Asterisk (*) indicates statistical significance ($p < 0.05$) and NS denotes non-significance

progression group (median PFS: training cohort, 13.4 months; validation cohort, 13.2 months). There was a significant difference in PFS between the two groups based on Kaplan–Meier survival curves (Fig. 4C, D) in both cohorts.

The time-dependent ROC curves (Fig. 4E, F) demonstrated that the proposed radiomics signature ($model_{all}$) was able to accurately and consistently predict the probability of disease progression at different time points. The AUCs at 6, 9, and 12 months ranged from 0.89 to 0.94 in the training cohort and 0.76 to 0.96 in the testing cohort.

Discussion

Disease progression is a turn of events for LUAD patients undergoing EGFR-TKI therapy due to the inevitable presence of acquired resistance to TKIs. However, the detection of progression often lags behind its occurrence in clinical practice and timely detection remains challenging. In our study, we proposed a radiomics signature that accounted for the intra- and peri-tumoral characteristics along with their variation between serial follow-up examinations. As the result, the novel imaging signature allowed for early progression prediction and risk stratification in LUAD patients treated with EGFR-TKIs, potentially offering valuable reference information to determine disease progression.

Our study demonstrated a robust performance of the radiomics signature as evidenced by the promising C-index in both cohorts (training cohort: 0.78, validation cohort: 0.72). The result suggested that the CT-based radiomics signature could be used as a prognostic predictor for LUAD patients

who received EGFR-TKI therapy. A multi-center study focusing on Stage IV EGFR-mutant NSCLC patients treated with EGFR-TKI therapy reported that the nomogram integrating pretherapy CT-based signature improved the prediction accuracy of PFS significantly [20]. A noteworthy difference from our work was the introduction of additional timepoint and our signature reflected the dynamic change of tumor heterogeneity. Tumor heterogeneity not only changes over time owing to subclonal diversities and genomic instability [36] but also alters between pre- and post-treatment under potent selective pressures arising from antineoplastic therapy, especially in targeted therapies [37, 38]. Fave et al discovered among 107 NSCLC patients during radiation therapy sessions that all radiomics features significantly changed from pretreatment CT imaging to subsequent weekly follow-ups [24]. Therefore, it could be insufficient to evaluate and predict individual progression status based on a single timepoint. Our study further confirmed that multi-timepoint radiomics signature outperformed the single-timepoint signature in PFS prediction in training cohort (C-index: 0.78 vs 0.66, p value < 0.001). The result highlighted the incremental value of dynamic tumor characteristics for this specific patient population.

Among the ten features constituting our radiomics signature, seven delta-radiomics features contributed crucial information associated with patient-specific outcome prediction. Previous studies presented controversy over the calculation and application of these delta-radiomics features. Nardone et al discovered delta-texture features were more robust than texture features through a phantom study [39]. A retrospective study of 107 NSCLC patients under radiotherapy revealed that
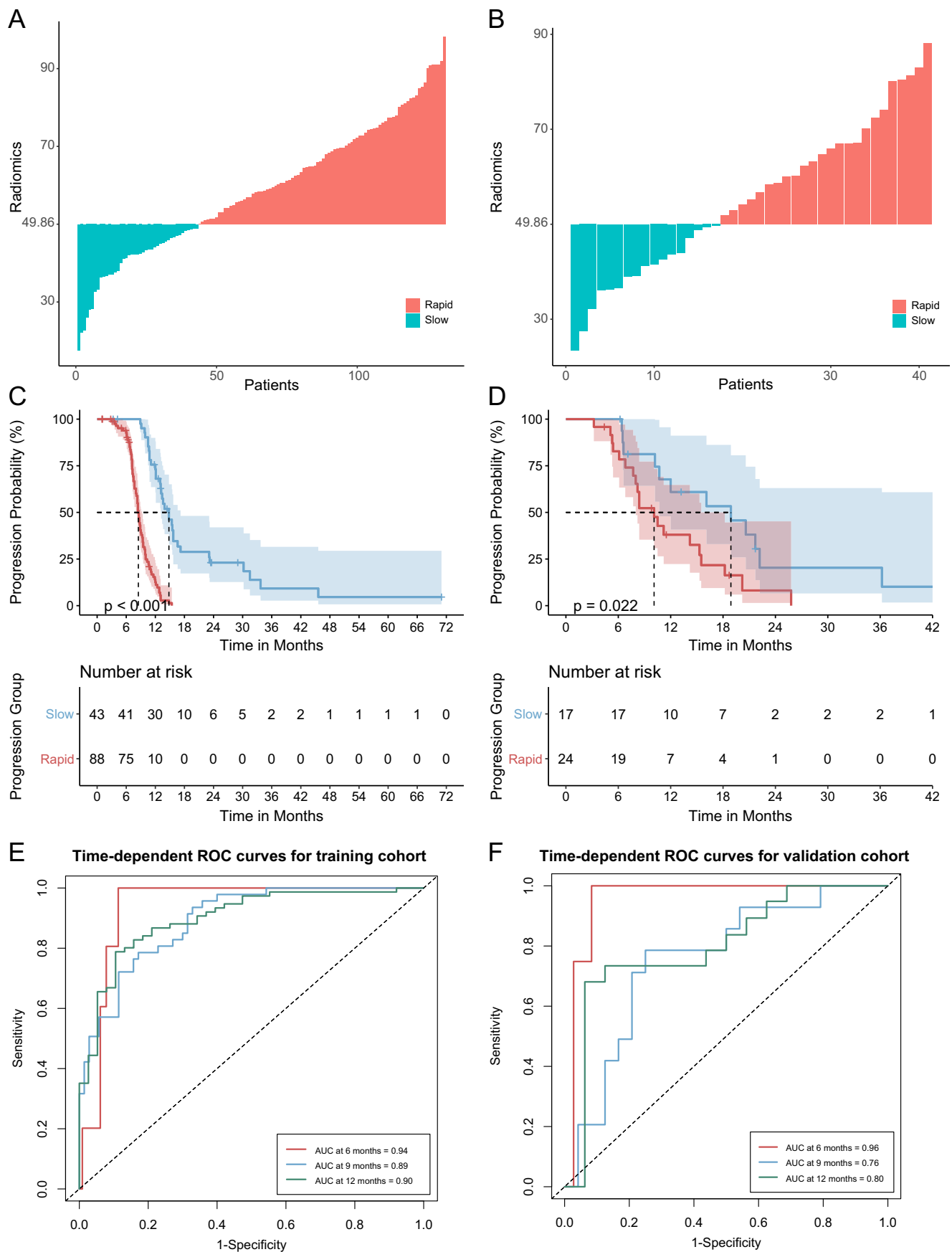
pretreatment imaging features were not prognostic, whereas delta-radiomics features had a statistically significant impact on estimation for local recurrence [24]. Contrarily in another smaller study consisting of 48 EGFR-mutant LUAD patients who received EGFR-TKIs, follow-up features were more predictive for PFS than the percentage change [21]. We suspected that different duration between therapy initiation and first follow-up imaging among patients could create bias. Therefore, we adjusted such factor by calculating the unit-time (per day) percentage change between the two timepoints, and our data indeed proved the prognostic value of these dynamic characteristics.

The interface between primary tumor and lung parenchyma offered clues to how tumor cells interact with recruited immune and stromal cell of the surrounding normal tissue [40–42]. Under such interplay, tumor cells acquired migratory phenotype and the capability of invading adjacent tissue [43–45]; therefore, capturing such phenotypic expression in the peritumoral regions could be beneficial. Our findings suggested the model integrating intra- and peritumoral features produced superior PFS predictive power over the intratumoral-alone model in training cohort (C-index: 0.78 vs 0.71, p value = 0.006). The prognostic benefit of peritumoral features was echoed by Dou et al in their study that peritumoral radiomics features were shown to have better prognostic performance compared to tumor radiomic signature for distant metastasis in patients with locally advanced NSCLC [26].

Baseline clinical characteristics exhibited weak association with progression status in the studied cohorts, as evidenced by the univariate analysis. The clinical model alone could not accurately predict PFS (C-index in training cohort: 0.55, validation cohort: 0.54); moreover, adding clinical characteristics to radiomics signature did not reveal any improvement. It suggested primary tumor volume at baseline was of limited value in prognostication of disease progression for LUAD patients undergoing EGFR-TKIs. Our result was consistent with several previous studies [20, 21] that baseline volume had a lower discriminative power in PFS estimation for EGFR-mutant LUAD patients receiving EGFR-TKIs compared with radiomics features.

The application of EGFR TKIs could result in different disease progression patterns and variable PFS. Kim et al [21] discovered that the PFS ranged from 0.3 to 29.4

months for the 48 enrolled lung adenocarcinoma patients treated with EGFR-TKI. Meanwhile, in another study, Song et al [20] found that the median PFS was 5.6 and 10.7 months for EGFR-TKI-treated NSCLC patients with rapid and slow progression, respectively. RECIST 1.1 assessment depends on the size change of the target lesion or appearance of new lesions, and disease progression can only be confirmed at the CT images on which progression has already occurred. The radiomics signature proposed in our study also accounted for lesion heterogeneity in the intratumoral and peritumoral space, along with their dynamic change throughout the course of therapy. As the result, we could make an early prognosis at the first follow-up imaging. We determined a cutoff value of the radiomics signature to stratify patients into rapid progression group (R-group) and slow progression groups (S-group). The stark survival contrast between groups potentially suggested personalized follow-up strategies; for instance, patients predictive of rapid progression may benefit from more positive and rigorous follow-up. The time-dependent ROC analysis further confirmed a favorable prognosis throughout the disease course, indicating accurate detection of progression and better re-biopsy timing selection.

There were some limitations in our study due to the inherent nature of its retrospective study. Firstly, the sample size was relatively small, particularly in the external validation cohort. Geographical variations also potentially introduced biases between the two studied cohorts. Our results need further verification on more large-scale cohorts. Secondly, CT imaging acquisition was derived from multiple institutes, different CT scanners, and protocols. The diagnostic efficacy of radiomics features can be influenced by the variability of CT acquisition and reconstruction parameters [46–51]. To alleviate the negative effect of scanner variability, we normalized slice thickness through $1 \times 1 \times 1$ mm resampling aiming to achieve more standardized feature extraction. Thirdly, unlike several previous studies, we analyzed non-contrast CT images rather than contrast-enhanced CT scans. Despite the added hemodynamic information, contrast agent could contaminate the biological heterogeneity within tumors depicted by radiomics features [46, 52]. Since NSCLC patients undergoing EGFR-TKI therapy require long-term follow-up, non-contrast CT may be more appropriate due to its high cost-effectiveness, strong reproducibility and controllable adverse effects and complications.

In conclusion, the proposed integrated radiomics signature was capable of capturing the dynamic information of intra- and peritumoral heterogeneity for LUAD patients who received EGFR-TKI therapy. This comprehensive imaging signature demonstrated considerably high potential in the prediction of disease progression and risk stratification. Once validated in larger cohorts, it is conducive to guide clinical decision-making such as personalized follow-up strategies.

Declarations

References

1. Shi Y, Au JS, Thongprasert S et al (2014) A prospective, molecular epidemiology study of EGFR mutations in Asian patients with advanced non-small-cell lung cancer of adenocarcinoma histology (PIONEER). J Thorac Oncol 9:154–162
2. Sequist LV, Yang JC-H, Yamamoto N et al (2013) Phase III study of afatinib or cisplatin plus pemetrexed in patients with metastatic lung adenocarcinoma with EGFR mutations. J Clin Oncol Official J Am Soc Clin Oncol 31:3327–3334
3. Mitsudomi T, Morita S, Yatabe Y et al (2010) Gefitinib versus cisplatin plus docetaxel in patients with non-small-cell lung cancer harbouring mutations of the epidermal growth factor receptor (WJTOG3405): an open label, randomised phase 3 trial. Lancet Oncol 11:121–128
4. Mok TS, Wu YL, Thongprasert S et al (2009) Gefitinib or carboplatin-paclitaxel in pulmonary adenocarcinoma. N Engl J Med 361:947–957
5. Maemondo M, Inoue A, Kobayashi K et al (2010) Gefitinib or chemotherapy for non-small-cell lung cancer with mutated EGFR. N Engl J Med 362:2380–2388
6. Rosell R, Carcereny E, Gervais R et al (2012) Erlotinib versus standard chemotherapy as first-line treatment for European patients with advanced EGFR mutation-positive non-small-cell lung cancer (EURTAC): a multicentre, open-label, randomised phase 3 trial. Lancet Oncol 13:239–246
7. Jekunen AP (2015) Role of Rebiopsy in Relapsed Non-Small Cell Lung Cancer for Directing Oncology Treatments. J Oncol 2015:1–11
8. Hasegawa T, Sawa T, Futamura Y et al (2015) Feasibility of Rebiopsy in Non-Small Cell Lung Cancer Treated with Epidermal Growth Factor Receptor-Tyrosine Kinase Inhibitors. Intern Med 54:1977–1980
9. Arcila ME, Oxnard GR, Nafa K et al (2011) Rebiopsy of lung cancer patients with acquired resistance to EGFR inhibitors and enhanced detection of the T790M mutation using a locked nucleic acid-based assay. Clin Cancer Res 17:1169–1180
10. Yu HA, Arcila ME, Rekhtman N et al (2013) Analysis of tumor specimens at the time of acquired resistance to EGFR-TKI therapy in 155 patients with EGFR-mutant lung cancers. Clin Cancer Res 19:2240–2247
11. Hata A, Katakami N, Yoshioka H et al (2013) Rebiopsy of non-small cell lung cancer patients with acquired resistance to epidermal growth factor receptor-tyrosine kinase inhibitor: comparison between T790M mutation-positive and mutation-negative populations. Cancer 119:4325–4332
12. Gillies RJ, Kinahan PE, Hricak H (2016) Radiomics: Images Are More than Pictures, They Are Data. Radiology 278:563–577
13. Lambin P, Rios-Velazquez E, Leijenaar R et al (2012) Radiomics: extracting more information from medical images using advanced feature analysis. Eur J Cancer 48:441–446
14. Lambin P, Leijenaar RTH, Deist TM et al (2017) Radiomics: the bridge between medical imaging and personalized medicine. Nat Rev Clin Oncol 14:749–762
15. Beig N, Khorrami M, Alilou M et al (2019) Perinodular and intranodular radiomic features on lung CT images distinguish adenocarcinomas from granulomas. Radiology 290:783–792
16. Hawkins S, Wang H, Liu Y et al (2016) Predicting malignant nodules from screening CT Scans. J Thorac Oncol 11:2120–2128
17. Khorrami M, Prasanna P, Gupta A et al (2020) Changes in CT radiomic features associated with lymphocyte distribution predict overall survival and response to immunotherapy in non-small cell lung cancer. Cancer Immunol Res 8:108–119
18. Coroller TP, Agrawal V, Narayan V et al (2016) Radiomic phenotype features predict pathological response in non-small cell lung cancer. Radiother Oncol 119:480–486
19. Aerts HJWL, Grossmann P, Tan Y et al (2016) Defining a radiomic response phenotype: a pilot study using targeted therapy in NSCLC Sci Rep 6:33860. https://doi.org/10.1038/srep33860
20. Song J, Shi J, Dong D et al (2018) A new approach to predict progression-free survival in stage IV EGFR-mutant NSCLC patients with EGFR-TKI therapy. Clin Cancer Res 24:3583–3592
21. Yang F, Kim H, Park CM et al (2017) The prognostic value of CT radiomic features for patients with pulmonary adenocarcinoma treated with EGFR tyrosine kinase inhibitors. PLoS One 12: e0187500
22. Li H, Zhang R, Wang S et al (2020) CT-based radiomic signature as a prognostic factor in stage IV ALK-positive non-small-cell lung cancer treated with TKI crizotinib: a proof-of-concept study. Front Oncol 10:57
23. Huang Y, Liu Z, He L et al (2016) Radiomics signature: a potential biomarker for the prediction of disease-free survival in early-stage (I or II) non-small cell lung cancer. Radiology 281:947–957

24. Fave X, Zhang L, Yang J et al (2017) Delta-radiomics features for the prediction of patient outcomes in non-small cell lung cancer. Sci Rep 7:588

25. Coroller TP, Grossmann P, Hou Y et al (2015) CT-based radiomic signature predicts distant metastasis in lung adenocarcinoma. Radiother Oncol 114:345–350

26. Lee H-S, Dou TH, Coroller TP, van Griethuysen JJM, Mak RH, Aerts HJWL (2018) Peritumoral radiomics features predict distant metastasis in locally advanced NSCLC. PLoS One 13:e0206108

27. Rios Velazquez E, Parmar C, Liu Y et al (2017) Somatic mutations drive distinct imaging phenotypes in lung cancer. Cancer Res 77: 3922–3930

28. Ozkan E, West A, Dedelow JA et al (2015) CT gray-level texture analysis as a quantitative imaging biomarker of epidermal growth factor receptor mutation status in adenocarcinoma of the lung. AJR Am J Roentgenol 205:1016–1025

29. Zhang L, Chen B, Liu X et al (2018) Quantitative biomarkers for prediction of epidermal growth factor receptor mutation in non-small cell lung cancer. Transl Oncol 11:94–101

30. Mei D, Luo Y, Wang Y, Gong J (2018) CT texture analysis of lung adenocarcinoma: can Radiomic features be surrogate biomarkers for EGFR mutation statuses. Cancer Imaging 18

31. Bak SH, Park H, Sohn I, Lee SH, Ahn MJ, Lee HY (2019) Prognostic impact of longitudinal monitoring of radiomic features in patients with advanced non-small cell lung cancer. Sci Rep 9: 8730

32. Hayes SA, Pietanza MC, O'Driscoll D et al (2016) Comparison of CT volumetric measurement with RECIST response in patients with lung cancer. Eur J Radiol 85:524–533

33. Eisenhauer EA, Therasse P, Bogaerts J et al (2009) New response evaluation criteria in solid tumours: revised RECIST guideline (version 1.1). Eur J Cancer 45:228–247

34. Cui Y, Yang W, Ren J et al (2021) Prognostic value of multiparametric MRI-based radiomics model: potential role for chemotherapeutic benefits in locally advanced rectal cancer. Radiother Oncol 154:161–169

35. Dong F, Li Q, Xu D et al (2019) Differentiation between pilocytic astrocytoma and glioblastoma: a decision tree model using contrast-enhanced magnetic resonance imaging-derived quantitative radiomic features. Eur Radiol 29:3968–3975

36. de Bruin EC, McGranahan N, Mitter R et al (2014) Spatial and temporal diversity in genomic instability processes defines lung cancer evolution. Science 346:251–256

37. Lloyd MC, Cunningham JJ, Bui MM, Gillies RJ, Brown JS, Gatenby RA (2016) Darwinian Dynamics of Intratumoral Heterogeneity: not solely random mutations but also variable environmental selection forces. Cancer Res 76:3136–3144

38. Dercle L, Fronheiser M, Lu L et al (2020) Identification of non-small cell lung cancer sensitive to systemic cancer therapies using radiomics. Clin Cancer Res 26:2151–2162

39. Nardone V, Reginelli A, Guida C et al (2020) Delta-radiomics increases multicentre reproducibility: a phantom study. Med Oncol 37:38

40. Quail DF, Joyce JA (2013) Microenvironmental regulation of tumor progression and metastasis. Nat Med 19:1423–1437

41. Gabrilovich DI, Ostrand-Rosenberg S, Bronte V (2012) Coordinated regulation of myeloid cells by tumours. Nat Rev Immunol 12:253–268

42. Condeelis J, Pollard JW (2006) Macrophages: obligate partners for tumor cell migration, invasion, and metastasis. Cell 124:263–266

43. van Zijl F, Mair M, Csiszar A et al (2009) Hepatic tumor-stroma crosstalk guides epithelial to mesenchymal transition at the tumor edge. Oncogene 28:4022–4033

44. Bhowmick NA, Neilson EG, Moses HL (2004) Stromal fibroblasts in cancer initiation and progression. Nature 432:332–337

45. Joyce JA, Pollard JW (2009) Microenvironmental regulation of metastasis. Nat Rev Cancer 9:239–252

46. He L, Huang Y, Ma Z, Liang C, Liang C, Liu Z (2016) Effects of contrast-enhancement, reconstruction slice thickness and convolution kernel on the diagnostic performance of radiomics signature in solitary pulmonary nodule. Sci Rep 6:34921. https://doi.org/10.1038/srep34921

47. Zhao B, Tan Y, Tsai W-Y et al (2016) Reproducibility of radiomics for deciphering tumor phenotype with imaging. Sci Rep 6:23428. https://doi.org/10.1038/srep23428

48. Berenguer R, Pastor-Juan MR, Canales-Vázquez J et al (2018) Radiomics of CT features may be nonreproducible and redundant: influence of CT acquisition parameters. Radiology 288:407–415

49. Li Y, Lu L, Xiao M et al (2018) CT slice thickness and convolution Kernel affect performance of a radiomic model for predicting EGFR status in non-small cell lung cancer: a preliminary study. Sci Rep 8:17913. https://doi.org/10.1038/s41598-018-36421-0

50. Shafiq-ul-Hassan M, Latifi K, Zhang G, Ullah G, Gillies R, Moros E (2018) Voxel size and gray level normalization of CT radiomic features in lung cancer. Sci Rep 8:10545. https://doi.org/10.1038/s41598-018-28895-9

51. Kim YJ, Lee H-J, Kim KG, Lee SH (2019) The effect of CT scan parameters on the measurement of CT radiomic features: a lung nodule phantom study. Comput Math Methods Med 2019:1–12

52. Goh V, Ganeshan B, Nathan P, Juttla JK, Vinayan A, Miles KA (2011) Assessment of response to tyrosine kinase inhibitors in metastatic renal cell cancer: CT texture as a predictive biomarker. Radiology 261:165–171